Crystallographic, X-ray Absorption, and IR Studies of Solid- and Solution-State Structures of Tris(nitrato) *N,N,N′,N′*-Tetraethylmalonamide Complexes of Lanthanides. Comparison with the Americium Complex

C. Den Auwer,*,†,‡ M. C. Charbonnel,† M. G. B. Drew,§ M. Grigoriev,||,⊥ M. J. Hudson,§ P. B. Iveson,§ C. Madic,# M. Nierlich,& M. T. Presson,† R. Revel,†,$ M. L. Russell,§ and P. Thuéry&

CEA Marcoule, DCC/DRRV/SEMP Laboratoire de Chimie Théorique et Structurale, 30207 Bagnols sur Cèze Cedex, France, Chemistry Department, University of Reading, Whiteknights, Reading RG6 6AD, U.K., Institute of Physical Chemistry of the Russian Academy of Sciences, 31 Leninsky Prosp., Moscow, Russia, CEA Saclay, DCC, 91191 Gif-sur-Yvette Cedex, France, and CEA Saclay, DSM/DRECAM/SCM (CNRS URA 331), 91191 Gif-sur-Yvette Cedex, France

Received July 9, 1999

To fine-tune the design of optimized donor ligands for nuclear waste actinide selective extraction, both electronic and molecular structures of the actinide complexes that are formed must be investigated. In particular, to achieve the selective complexation of transplutonium 3+ ions versus lanthanide 3+ ions is one of the major challenges, given the chemical similarities between these two f-element families. In this work, the structure of solvent-phase $M(NO_3)_3(TEMA)_2$ complexes (Ln = Nd, Eu, Ho, Yb, Lu, Am; TEMA = *N,N,N′,N′*-tetraethylmalonamide) was investigated by liquid-phase spectroscopic methods among which extended X-ray absorption fine structure played a major role. In addition, the crystal structures of the species $Nd(NO_3)_3(TEMA)_2$ and $Yb(NO_3)_3(TEMA)_2$ have been determined by X-ray diffraction. $Nd(NO_3)_3(C_{11}N_2O_2H_{22})_2$ crystallizes in the monoclinic system ($P2_1$ space group; $a = 11.2627(4)$ Å, $b = 20.5992(8)$ Å, $c = 22.2126(8)$ Å; $\alpha = \gamma = 90°$, $\beta = 102.572(1)°$; $Z = 6$), and $Yb(NO_3)_3(C_{11}N_2O_2H_{22})_2$ crystallizes in the orthorhombic system ($P2_12_12_1$ space group; $a = 9.3542(1)$ Å, $b = 18.1148(2)$ Å, $c = 19.7675(2)$ Å; $\alpha = \beta = \gamma = 90°$; $Z = 4$). In the solvent phase, the metal polyhedron was found to be similar to that of the solid-state complex $Nd(NO_3)_3(TEMA)_2$ for M = Nd to Ho. For M = Yb and Lu, a significant elongation of one nitrate oxygen bond was observed. Comparison with measurements on the $Am(NO_3)_3(TEMA)_2$ complex in ethanol has shown the similarities between the Nd^{3+} and Am^{3+} coordination spheres.

Introduction

Actinide coordination chemistry is well-known for its richness, which is a consequence of the large variety of oxidation states that are available, especially for the light actinides.[1] However for the actinide elements heavier than plutonium, ionic 3+ character is most often found such that properties are similar to those of the lanthanide elements.[2,3] Although numerous review articles have covered 4f-element physical chemistry,[4,5] very few publications have dealt with transplutonium coordination structural chemistry, due to both little research because of major safety concerns and the low availability of these elements.[6] The majority of actinide structural chemistry studies have been triggered by environmental concerns. Nuclear waste disposal,[7,8] contaminated soil remediation,[9,10] and selective ion extraction during nuclear fuel reprocessing[11−13] are some examples in which actinide structural chemistry has found application. In the case of decontamination or selective extraction problems, well-adapted ligands have to be conceived for selective complexation purposes.[14] One of the major challenges

† CEA Marcoule.
‡ LURE, Université Paris-Sud, 91898 Orsay Cedex, France (affiliate researcher).
§ University of Reading.
|| Institute of Physical Chemistry of the Russian Academy of Sciences.
⊥ Visiting scientist at CEA Marcoule.
CEA Saclay DCC.
& CEA Saclay, DSM/DRECAM/SCM.
$ Present address: Institut Français du Pétrole, 1-4 av. de Bois-Préau, 92852 Rueil Malmaison cedex, France.

(1) Choppin, G. R.; Liljenzin, J.; Rydberg, J., *Radiochemistry and Nuclear Chemistry*; Butterworths-Heinemann: Oxford, U.K., 1995.
(2) Bartenev, S. A.; Markov, G. S.; Romanovskii, V. N.; Khramov, N. N. *Radiochemistry* **1998**, *40*, 3.
(3) Seaborg, G. T., *Radiochem. Acta* **1993**, *61*, 115.
(4) Gschneidner, K. A.; Eyring, L. *Handbook on the Physics and Chemistry of Rare Earth*; Elsevier: Amsterdam, 1996; Vol. 22.
(5) Bagnall, K. W. *MTP International Review of Science*; Inorganic Chemistry Series 1&2; Butterworths: London, 1972; Vol. 7.
(6) Bagnall, K. W. The Actinides. In *Comprehensive Coordination Chemistry*; Wilkinson, G., Ed.; Pergamon Press: Oxford, U.K., 1987; Vol. 7.
(7) Brookins, D. G.; *The Geological Disposal of High Level Radioactive Wastes*; Theophrastus: Zographou, Athens, Greece, 1987.
(8) Barré, J. Y. The Future of the Back End of the Fuel Cycle. *Mater. Res. Soc. Symp. Proc.* **1992**, *257*.
(9) Philips, E. J. P.; Landa, E.; Lovely, D. R. *J. Ind. Microbiol.* **1995**, *14*, 203.
(10) Jacobs, R. A.; Sengun, M. Z.; Hicks, R. E.; Probstein, R. S. *J. Environ. Sci. Health* **1994**, *A29*, 1933.
(11) Schulz, W. W.; Burger, L. L.; Navratil, J. D. *Science and Technology of Tributyl Phosphate*; CRC Press: Boca Raton, FL, 1990; Vol. III.
(12) Muramaya, T.; Kubota, M.; Takizuka, T.; Ogawa, T.; Mizumoto, M.; Yoshida, H. Proceedings of the GLOBAL'95 Conference, Versailles, France, 1995; Vol. I, p 110.
(13) Viala, M.; Salvatores, M. Proceedings of the GLOBAL'95 Conference, Versailles, France, 1995; Vol. I, p 118.

10.1021/ic990817x CCC: $19.00
Published on Web 03/16/2000

is then to evaluate the structure/reactivity relationship in order to fine-tune the design of the most favorable ligand for the required process. For that purpose, both electronic and molecular structures of the species need to be understood. X-ray diffraction is one of the major tools for actinide compound structural investigation and comparison with lanthanide analogues.[15] Other techniques such as infrared spectroscopy, nuclear magnetic resonance,[16,17] and fluorescence spectroscopy[18,19] have also been used in order to characterize the actinide coordination sphere. However, in the field of actinide solvent extraction, the species of interest are located in the solvent phase and solid-state investigation methods, although necessary, are of partial use. This is why extended X-ray absorption fine structure (EXAFS) has become of primary importance lately.[20] Although numerous papers have dealt with U, Np, and Pu coordination complexes,[21−33] very few have reported studies on complexes of transplutonium elements.[34−36]

Our group has been working in the field of 4f and 5f solvent-phase coordination chemistry related to the selective solvent extraction processes of used nuclear fuels.[14,37,38] In particular, various studies have been devoted to the complexation ability of oxygen donor ligands.[21−23,39−41] However, to our knowledge, no structural comparison of solvent-phase coordination complexes of 4f and transplutonium elements has been reported to date and we present here our first results on tris(nitrato)-lanthanide and -americium adducts with the *N*,*N*,*N*′,*N*′-tetraethylmalonamide (TEMA) ligand. More precisely, we focus in this paper on the structural evolution of the metal coordination sphere within the series of $M^{3+}(NO_3^-)_3(TEMA)_2$ (M = Nd, Eu, Ho, Yb, Lu, Am) complexes in ethanol or methanol.

Experimental Section

(a) Syntheses. The TEMA malonamide was provided by Panchim Co., Lisses 91, France, with a purity better than 98%. Hydrated lanthanide nitrates ($Nd(NO_3)_3 \cdot 6H_2O$ from Prolabo Rectapur, $Eu(NO_3)_3 \cdot 6H_2O$ from Strem Chemicals, $Ho(NO_3)_3 \cdot 6H_2O$ from Aldrich Chemicals, $Yb(NO_3)_3 \cdot 5H_2O$ and $Lu(NO_3)_3 \cdot 5H_2O$ from Alfa) were dissolved in absolute ethanol (Prolabo).

Single-Crystal Sample Preparation. Complex 1, $Nd(NO_3)_3(TEMA)_2$. The complex was first obtained as a powder by reaction of a 0.2 M solution of $Nd(NO_3)_3.6H_2O$ in ethanol with a 0.4 M solution of TEMA in ethanol. After a few hours, we obtained a pink precipitate. This filtered precipitate was then recrystallized in ethanol. Anal. Calcd for $NdC_{22}N_7O_{13}H_{44}$: Nd, 19.0; C, 34.8; N, 12.9. Found: Nd, 21.4; C, 30.9; N, 10.8. H and O were not determined.

Complex 2, $Yb(NO_3)_3(TEMA)_2$. The complex was synthesized in the same way as for complex **1**. Recrystallization from 2-propanol around 5 °C gave colorless single crystals suitable for X-ray crystallography. Crystals with the same structure but of poorer quality have been obtained from ethanol solution. Anal. Calcd for $YbC_{22}N_7O_{13}H_{44}$: Yb, 22.0; C, 33.5; N, 12.5. Found: Yb, 24.8; C, 33.0; N, 12.3. H and O were not determined.

Solution Sample Preparation. Lanthanide Complexes. Bis(malonamide) complexes were prepared by dissolving 0.001 mol of Ln^{3+} (Ln = Nd, Ho, Yb, Lu) in 5 mL of TEMA (0.4 mol/L) in absolute ethanol. All solutions have been found to be metastable versus precipitation within a few days. In the case of the Eu ion, to avoid the precipitation of the complex that occurred after few minutes in ethanol, methanol has been used. The final composition of the organic phase was checked by diamide and Ln titration with $HClO_4$ in acetic medium and colorimetry with arsenazo(III), respectively.

Americium Complex. An 8 mg portion of $^{241}AmO_2$ was dissolved in 2 mL of HNO_3 (5 mol/L). The solution was then slowly evaporated to eliminate the excess nitric acid and cooled to room temperature just before dryness. A 1 mL amount of TEMA (0.12 mol/L) was then added to give a pale yellow solution in ethanol. Complexation of the TEMA ligand to the Am metal was checked by IR spectroscopy: $\nu_{C=O}$(ligand) band at 1614.5 cm^{-1}.

(b) IR Spectra. The FTIR spectra of the solution samples were recorded on a Nicolet Magna 550 spectrometer. For the 4000−650 cm^{-1} spectral range, 0.2 mL of solution was deposited on a ZnSe attenuated total reflectance (ATR) crystal. For the 500−100 cm^{-1} range, 10 mL of solution was deposited onto a 3 M polyethylene film under a dry N_2 atmosphere. IR vibration bands for the lanthanide and americium complexes are given in Table 1.

(c) Crystal Structures. The structures of $Nd(NO_3)_3(TEMA)_2$ (**1**) and $Yb(NO_3)_3(TEMA)_2$ (**2**) were determined. Data were collected on a Nonius Kappa-CCD area detector diffractometer using graphite-monochromated Mo Kα radiation (0.710 73 Å). The crystals were introduced into Lindemann glass capillaries. The lattice parameters were determined from 10 images recorded with 1° ϕ scans and later refined on all data. A 180° ϕ range was scanned with 2° steps during data recording for **1** and one-eighth of the reciprocal space with 0.35° steps in ϕ or ω for **2**.[42] The crystal-to-detector distance was fixed at 29 mm.

(14) Madic, C.; Hudson, M. J. *High-Level Liquid Waste Partitioning by Means of Completely Incinerable Extractants*; European Commission, Nuclear Science and Technology; EUR 18038 EN, Luxembourg, 1998.
(15) See for instance: Grigor'ev, M. S.; Charushnikova, I. A.; Krot, N. N.; Yanovskii, A. I.; Struchkov, Yu, T. *Radiochemistry* **1997**, *39*, 420.
(16) Berthon, C.; Chachaty, C. *Solvent Extr. Ion Exch.* **1995**, *13*, 781.
(17) Meinrath, G. *J. Radioanal. Nucl. Chem. Lett.* **1994**, *186*, 257.
(18) Thouvenot, P.; Hubert, S.; Moulin, C.; Decambox, P.; Mauchlen, P. *Radiochim. Acta* **1993**, *61*, 15.
(19) Kim, J. I.; Wimmer, H.; Klenze, R. *Radiochim. Acta* **1991**, *54*, 35.
(20) Conradson, S. D. *Appl. Spectrosc.* **1998**, *52*, 252.
(21) Den Auwer, C.; Charbonnel, M. C.; Presson, M. T.; Madic, C.; Guillaumont, R. *Polyhedron* **1998**, *17*, 4507.
(22) Den Auwer, C.; Lecouteux, C.; Charbonnel, M. C.; Madic, C.; Guillaumont, R. *Polyhedron* **1997**, *16*, 2233.
(23) Den Auwer, C.; Revel, R.; Charbonnel, M. C.; Presson, M. T.; Conradson, S. D.; Simoni, E.; Le Du, J. F.; Madic, C. *J. Synchrotron Radiat.* **1999**, *6*, 101.
(24) Clark, D. L.; Conradson, S. D.; Keogh, D. W.; Palmer, P. D.; Scott, B. L.; Tait, C. D. *Inorg. Chem.* **1998**, *37*, 2893.
(25) Clark, D. L.; Hobart, D. E.; Neu, M. P. *Chem. Rev.* **1995**, *95*, 25.
(26) Clark, D. L.; Conradson, S. D.; Neu, M. P.; Palmer, P. D.; Runde, W.; Tait, C. D. *J. Am. Chem. Soc.* **1997**, *119*, 5259.
(27) Clark, D. L.; Conradson, S. D.; Ekberg, S. A.; Hess, N. J.; Neu, M. P.; Palmer, P. D.; Runde, W.; Tait, C. D. *J. Am. Chem. Soc.* **1996**, *118*, 2089.
(28) Clark, D. L.; Conradson, S. D.; Ekberg, S. A.; Hess, N. J.; Janecky, D. R.; Neu, M. P.; Palmer, P. D.; Tait, C. D. *New J. Chem.* **1996**, *20*, 211.
(29) Reich, T.; Moll, H.; Arnold, T.; Denecke, M. A.; Hennig, C.; Geipel, G.; Bernhard, G.; Nitsche, H.; Allen, P. G.; Bucher, J. J.; Edelstein, N. M.; Shuh, D. K. *J. Electron Spectrosc. Relat. Phenom.* **1998**, *96*, 237.
(30) Allen, P. G.; Bucher, J. J.; Shuh, D. K., Edelstein, N. M.; Reich, T. *Inorg. Chem.* **1997**, *36*, 4676.
(31) Allen, P. G.; Veirs, D. K.; Conradson, S. D.; Smith, C. A.; Marsh, S. F. *Inorg. Chem.* **1996**, *35*, 2841.
(32) Karim, D. P.; Georgopoulos, P.; Knapp, G. S. *Nucl. Technol.* **1980**, *51*, 162.
(33) Veirs, D. K.; Smith, C. A.; Berg, J. M.; Zwick, B. D.; Marsh, S. F.; Allen, P.; Conradson, S. *J. Alloys Compd.* **1994**, *213&214*, 328.
(34) Soderholm, L.; Williams, C.; Skanthakumar, S.; Antonio, M. R.; Conradson, S. *Z. Phys. B: Condens. Matter* **1996**, *101*, 539.
(35) Soderholm, L.; Skanthakumar, S.; Staub, U.; Antonio, M. R.; Williams, C. W. *J. Alloys Compd.* **1997**, *250*, 623.
(36) Revel, R.; Den Auwer, C.; Madic, C.; David, F.; Fourest, B.; Hubert, S.; Le Du, J. F.; Morss, L. R. *Inorg. Chem.* **1999**, *38*, 4139.
(37) Kolarik, Z.; Müllich, U.; Gassner, F. *Solvent Extr. Ion Exch.* **1999**, *17*, 23.
(38) Guilbaud, P.; Wipff, G. *J. Mol. Struct. (THEOCHEM)* **1996**, *366*, 55.
(39) Guilbaud, P.; Varnek, A.; Wipff, G. *J. Am. Chem. Soc.* **1993**, *115*, 8298.
(40) Guilbaud, P.; Dognon, J. P., *Proceedings of the 5th International Information Exchange Meeting*; Mol, Belgium; OECD-NEA Publications: Paris, France, 1999; EUR 18898 EN.
(41) Rabbe, C.; Sella, C.; Madic, C.; Godard, A. *Solvent Extr. Ion Exch.* **1999**, *17*, 87.
(42) COLLECT: Data Collection Software; Nonius BV, Delft, The Netherlands, 1998.

Table 1. Infrared Vibration Bands (cm^{-1}) for $Ln(NO_3)_3(TEMA)_2$ and $Am(NO_3)_3(TEMA)_2$ Complexes (0.2 mol/L in Ethanol)

free TEMA	Ln				Am	assignt[a]
	Nd	Ho	Yb	Lu		
1628	1615	1620	1620.5	1621	1614.5	$\nu_{C=O}$ stretch
	1590	1594	1593.6	1594	1590.5	$\nu'_{C=O}$
	1474	1475	1479	1479		ν_4 NO_3^- asym NO_2 stretch
	1302	1286	1301	1298		ν_1 NO_3^- sym NO_2 stretch
	818	816	816	816		ν_6 NO_3^- out of plane rock
	737	745	749	751		ν_3 NO_3^- sym $\delta(NO_2)$
	207	208	211	214		ν_{Ln-O} stretch
	172	189	178	181		$\Delta\nu_4-\nu_1$

[a] Tentative assignments according to the literature referred in the text.

Table 2. Crystallographic Data for 1, $Nd(NO_3)_3(TEMA)_2$

chem formula: $C_{22}H_{44}NdN_7O_{13}$	fw = 758.88
$a = 11.2627(4)$ Å	space group: $P2_1$ (No. 4)
$b = 20.5992(8)$ Å	$T = 293(2)$ K
$c = 22.2126(8)$ Å	$\lambda = 0.710\ 73$ Å
$\alpha = \gamma = 90°$	$\rho_{calcd} = 1.503$ g cm^{-3}
$\beta = 102.572(1)°$	$\mu = 16.15$ cm^{-1}
$V = 5030(2)$ Å^3	$R(F_o)^a = 0.035$
$Z = 6$	$R_w(F_o^2)^a = 0.082$

[a] $R(F_o) = \sum||F_o| - |F_c||/\sum|F_o|$; $R_w(F_o^2) = \{\sum[w(F_o^2 - F_c^2)^2]/[\sum F_o^4]\}^{1/2}$.

Table 3. Crystallographic Data for 2, $Yb(NO_3)_3(TEMA)_2$

chem formula: $C_{22}H_{44}YbN_7O_{13}$	fw = 787.68
$a = 9.3542(1)$ Å	space group: $P2_12_12_1$ (No. 19)
$b = 18.1148(2)$ Å	$T = 293(2)$ K
$c = 19.7675(2)$ Å	$\lambda = 0.710\ 73$ Å
$\alpha = \beta = \gamma = 90°$	$\rho_{calcd} = 1.562$ g cm^{-3}
$V = 3349.59(6)$ Å^3	$\mu = 28.59$ cm^{-1}
$Z = 4$	$R(F_o)^a = 0.018$
	$R_w(F_o)^a = 0.041$

[a] See footnote *a* of Table 2.

The data were processed with the HKL package.[43] The structures were solved by the heavy-atom method with SHELXS-86[44] and subsequent Fourier-difference syntheses and refined by full-matrix least squares on F^2 with SHELXL-93.[45] Absorption effects were empirically corrected with the program MULABS from PLATON.[46] An important disorder is present in the aliphatic chains in the structure of **1** (seven disordered atoms), whereas there is no disorder in **2**. The disordered atoms have been modeled by two alternative positions with refined occupation factors constrained to sum up to unity. All non-hydrogen atoms were refined anisotropically, with the exception of the disordered ones. The hydrogen atoms were introduced (except for the disordered parts) as riding atoms with a displacement parameter equal to 1.2 (CH_2) or 1.5 (CH_3) times that of the attached carbon atom. Analytical scattering factors for neutral atoms were corrected for the anomalous dispersion terms $\Delta f'$ and $\Delta f''$. The correct enantiomorphs were determined from the Flack parameter (−0.002(13) and −0.009(5) in **1** and **2**, respectively).[47] Details of the crystallographic data are given in Tables 2 and 3. R1 = $\sum||F_o| - |F_c||/\sum|F_o|$, calculated on "observed" ($I > 2\sigma(I)$) reflections; wR2 = $\{\sum[w(F_o^2 - F_c^2)^2]/\sum wF_o^4]\}^{1/2}$ with $w = [\sigma^2(F_o^2) + (xP)^2 + yP]^{-1}$, where $P = (F_o^2 + 2F_c^2)/3$ and x and y are refined values; $S = \{\sum[w(F_o^2 - F_c^2)^2]/(n - p)\}^{1/2}$, where n and p are the number of reflections and the number of parameters refined, respectively. The molecular drawings were done with SHELXTL.[48] All calculations were performed with Silicon Graphics R5000 workstations at the CEA Saclay and CEA Marcoule.

(d) XAS Measurements. Data Collection. X-ray absorption spectra were recorded on complex **1** in the solid state and complexes $M(NO_3)_3(TEMA)_2$ (M = Nd, Eu, Ho, Yb, Lu, Am) in the solvent phase.

XAS data at the lanthanide (Ln) and americium L_{III} edges were recorded both at the LURE (Laboratoire pour l'Utilisation du Rayonnement Electromagnétique) facility on the DCI ring and at the Daresbury National Laboratory. On the DCI ring, the D44 experimental station was used with a double-crystal Si(111) monochromator for the Ln edges and Si(311) for the Am edge. At the Ln edges, harmonic rejection was achieved by detuning the crystals by 30%. Energy calibration was carried out by using Cr foil (at 5994.6 eV) for the Nd edge, Fe foil (at 7131.3 eV) for the Eu edge, Ni foil (at 8350.0 eV) for the Ho edge, Cu foil (at 8993.9 eV) for the Lu edge, and Zr foil (at 18014 eV) for the Am edge. All the characteristic edge features used for the above calibrations are calibrated toward the edge inflection point according to ref 49. Ionization chambers filled with air (Ln edges) and Ar (Am edge) were used for transmission mode detection. The energy resolution was 2.0, 2.7, 3.6, and 4.7 eV at the Nd (6208 eV), Eu (6977 eV), Ho (8071 eV), and Lu (9244 eV) edges, respectively, and 8.0 eV at the Am (18504 eV) edge. On the Daresbury ring, experimental station 7.1 was used with a double-crystal Si(111) monochromator for the Ln edges. At the Ln edges, harmonic rejection was achieved by detuning the crystals by 30%. Energy calibration was carried out by using Mn foil (at 6538 eV) for the Nd edge and Cu foil (at 8993.9 eV) for the Yb edge.[49] Ionization chambers filled with an air−He mixture were used for transmission mode detection. The energy resolution was 2.0 and 4.4 eV at the Nd (6208 eV) and Yb (8944 eV) edges, respectively.

Data Treatment. Data treatment was carried out by using the EXAFSPOWER code.[50] The pre-edge region was removed by using a linear function defined by two points on the pre-edge. Atomic absorption was modeled by using a third-degree polynomial function (coefficients determined by a least-squares fit). Following Lengeler and Eisenberger normalization, EXAFS oscillations were Fourier-transformed (FT) using a Kaiser window ($\tau = 2.5$) between 2.5 and 11.0 Å^{-1}. Filtering of the first coordination sphere (region **I**) was achieved by back Fourier transformation between 1.3 and 3.0 Å.

Data Fitting. The designation of model compounds is a crucial prerequisite for the interpretation of any EXAFS spectroscopy results. Such a procedure is indispensable for the extraction of experimental electronic parameters (backscattering phases $\Phi(\theta, k, R)$, amplitudes $f(\theta, k, R)$, electron mean free path $\lambda(k)$, and inelastic losses $\mathbf{S_0^2}$) that are required in the fitting of the spectra of unknown compounds. However, this way of evaluating the backscattering phases and amplitudes does not allow for the independent fitting of the various neigbhor contributions (i.e. the various photoelectron paths), when the latter are not perfectly deconvoluted in the pseudo-radial distribution function (obtained by Fourier transformation of the EXAFS oscillations). This is the case of the present system, given that the EXAFS resolution ($\Delta R = \pi/2\Delta k$, where R is the M−O distance and Δk is the FT window range) is equal to 0.18 Å, while the difference between the shortest and the longest contributions of region I is 0.25 Å (cf. Table 4). An alternative method consists of using semiempirical codes that can be used to calculate these electronic functions for each photoelectron path. This method, however, requires the input of the atomic positions of a model compound and careful use of the independent scattering paths. Here, complex **1**, i.e. $Nd(NO_3)_3(TEMA)_2$ in the solid state, has been taken as the model compound for the EXAFS analysis of the $M(NO_3)_3(TEMA)_2$ series, and its EXAFS spectrum has

(43) Otwinowski, Z.; Minor, W. Processing of X-ray Diffraction Data Collected in Oscillation Mode. In *Methods in Enzymology*; Carter, C. W., Jr., Sweet, R. M., Eds.; Academic Press: New York, 1997; Vol. 276 (Macromolecular Crystallography, Part A), p 307.
(44) Sheldrick, G. M. *Acta Crystallogr., Sect. A* **1990**, *46*, 467.
(45) Sheldrick, G. M. SHELXL-93: Program for the Refinement of Crystal Structures; University of Göttingen, Göttingen, Germany, 1993.
(46) Spek, A. L. PLATON; University of Utrecht, Utrecht, The Netherlands, 1998.
(47) Flack, H. D. *Acta Crystallogr., Sect. A* **1983**, *39*, 876.
(48) Sheldrick, G. M. SHELXTL; University of Göttingen, Göttingen, Germany (distributed by Bruker AXS, Madison, WI), 1997.
(49) *Reference X-ray Spectra of Metal Foils*; EXAFS MATERIALS: 871 El Cerro Blvd., Danville, CA 94526. See also: Bearden, J. A.; Burr, A. F. *Rev. Mod. Phys.* **1967**, *39*, 125.
(50) Michalowicz, A. *J. Phys. IV* **1997**, *7*, C2−235. Available on the LURE web site: www.lure.u-psud.fr. See also: Michalowicz, A. Thèse de l'Université Paris, Val de Marne, France, 1990.

Table 4. Selected Distances (Å) and Torsion Angles (deg) in **1** and **2**

	1			
	A	B	C	**2**
Metal Ion Environment				
M^{3+}−O(TEMA)				
O(1)	2.435(6)	2.438(6)	2.443(6)	2.297(2)
O(2)	2.439(6)	2.446(7)	2.430(7)	2.293(2)
O(3)	2.452(7)	2.444(7)	2.427(7)	2.292(2)
O(4)	2.432(6)	2.448(6)	2.454(6)	2.280(2)
M^{3+}−O(nitrate)				
O(11)	2.574(6)	2.632(8)	2.663(9)	2.485(2)
O(12)	2.677(7)	2.560(8)	2.530(8)	2.447(2)
O(21)	2.569(6)	2.679(8)	2.573(7)	2.315(2)
O(22)	2.669(6)	2.590(7)	2.700(7)	
O(31)	2.512(8)	2.557(7)	2.570(7)	2.414(2)
O(32)	2.524(8)	2.541(7)	2.522(7)	2.458(2)
Ligand Geometry				
O(1)···O(2)	2.850(9)	2.787(8)	2.774(9)	2.702(2)
O(3)···O(4)	2.809(9)	2.755(9)	2.726(9)	2.652(2)
C(8)−N(5)−C(1)−C(2)	4.2	168.5	169.6	−1.0
N(5)−C(1)−C(2)−C(3)	133.2	132.8	126.8	129.4
C(1)−C(2)−C(3)−N(4)	−107.0	−173.4	−170.4	−143.6
C(2)−C(3)−N(4)−C(4)	174.1	−2.9	−1.9	−178.9
C(19)−N(7)−C(12)−C(13)	178.7	−4.3	−3.4	−176.2
N(7)−C(12)−C(13)−C(14)	142.7	−140.3	−145.1	−166.2
C(12)−C(13)−C(14)−N(6)	−112.4	−173.8	−171.6	−172.7
C(13)−C(14)−N(6)−C(15)	−0.4	−164.2	167.7	4.5
O(1)−C(1)···C(3)−O(2)	14.9	−35.2	−36.9	−12.5
O(3)−C(12)···C(14)−O(4)	24.2	41.9	40.3	22.8

been simulated by the FEFF702[51] code. Two regions are present in the FT: region **I** for the first coordination sphere and region **II** for the further spheres. As discussed in the EXAFS section, region **I** mainly contains 10 contributions from the 10 oxygen neigbhors of the metal (3 bidentate nitrates, M−O(nitrate), and 2 bidentate malonamides, M−O(ligand)). It also accounts for the 3 single-scattering metal to nitrogen M···N(nitrate) contributions as well as for several multiple-scattering metal to carbon contributions. Averaging the three crystallographically independent molecules in **1** did not improve the simulation, and thus, only molecule A was taken into account in the FEFF input file (simulation of region **II** of the FT was improved by averaging the three units, but this tedious work is beyond the scope of this paper). The FEFF parameters were as follows: maximum number of scattering legs 5, maximum scattering length 7 Å, exchange correlation potential Hedin−Lundqvist, energy threshold shift −11 eV, plane wave filter 1.2%, curved wave filter 1.4%.

Fitting of the filtered region **I** EXAFS oscillations was carried out using two methods. Errors were estimated after determination of the data standard deviation, $s(k)$, in CHI(k) and k*CHI(k) using the STATEXAFS[52] code.

Method A. Since region **I** accounts for several nondeconvoluted contributions, it was first fitted with Round Midnight code[50] using a one-shell approximation. Electronic parameters of this unique shell (the phase $\Phi(\pi, k, R)$, amplitude $f(\pi, k, R)$ and electron mean free path $\lambda(k)$) were obtained by back-Fourier transformation (1.3−3.0 Å) of the FEFF simulated spectrum of **1**. Correct adjustment of filtered region **I** was possible when only the 10 M−O single-scattering contributions were considered. All the other contributions cancel each other because of phase opposition and should not be included in the fit. Fits were carried out in k[CHI(k)] with $1/s(k)^2$ weighting on the filtered oscillations (where $s(k)$ is the standard deviation of the EXAFS data; only its mean, s, is given in Table 5).

Method B. While method A is the classical fitting procedure, it gives limited information on the structure of the metal polyhedron. We propose here an experimental method that should be viewed as a way of looking at structural evolutions within a series, given that the starting structure is perfectly known and is not assumed to be significantly modified across the series. The phases $\Phi(\pi, k, R)$, amplitudes $f(\pi, k, R)$, and electron mean free path $\lambda(k)$ of each of the 10 single scattering M−O paths were extracted from the above FEFF simulation of **1**. The adjustments were carried out in CHI(k) with $1/s^2$ weighting on the filtered oscillations using the FEFFIT[51,53,54] code. Best fit results for method B are given in Table 6.

For all liquid samples, fits were carried out according to both methods. The number of neighbors was never allowed to vary and was set to 10 (adjusting this parameter would lead to unsignificant fit results, given the large uncertainty on this amplitude parameter). Fitted parameters were the energy threshold e_0, S_o^2, the Debye−Waller factor σ^2, and R. Strictly speaking, S_o^2 accounts here for the product of the inelastic losses $\mathbf{S_0^2}$ by the errors in the calculation of the amplitude functions ($f(\pi, k, R)$ and $\lambda(k)$). It was always allowed to vary in the same time as another parameter. For method A, R and σ or e_0 and σ were fitted together with S_0^2. For method B, two Debye−Waller factors were considered, one for the six Nd−O(nitrate) bonds and one for the four Nd−O(amide) bonds. For better comparison within the series, the two Debye−Waller factors were kept equal for all liquid samples. Only one distance R was allowed to vary in the same time, and in all cases, only one parameter plus S_o^2 were freed. The fitting procedure was repeated until all the variables stabilized from one fit cycle to another.

For each complex, the potential of the absorbing atom (Nd, Eu, Ho, Yb, Lu, Am) was recalculated by the FEFF code (by changing the lanthanide atomic number, Z_{Ln}, in the input file) in order to get the electronic functions corresponding to the fitted lanthanide.[56]

First, to validate the fitting procedures, the filtered EXAFS spectrum (region **I**) of solid-state model compound **1** was fitted. Method A: $S_0^2 = 1.20 \pm 0.02$, $N = 10$ (fixed), $R = 2.54 \pm 0.01$ Å, $\sigma^2 = 0.0009 \pm 0.0001$ Å^2 and $e_0 = 0.76 \pm 0.01$ eV compared to $R = 2.53$ Å given by the diffraction structure of Table 4. The r factor of the fit was equal to 0.01.[50] Method B: $S_0^2 = 0.97 \pm 0.05$; $R = 2.41, 2.43, 2.44, 2.45, 2.53, 2.53, 2.57, 2.59, 2.66, 2.67$ Å (all ± 0.01) and $e_0 = -0.19 \pm 0.42$ eV compared to 2.43, 2.44, 2.44, 2.45, 2.51, 2.52, 2.57, 2.57, 2.67, 2.68 Å given by the diffraction structure in Table 4. σ^2(nitrate) $= 0.0005 \pm 0.0005$ Å^2; σ^2(ligand) $= 0.0010 \pm 0.0004$ Å^2. The r factor[55] of the fit was equal to 0.017.

In the following results of method B, the four oxygen atom distances from the two amide ligands were averaged, since there was negligible divergence (∼0.02 Å) across the series within these distances.

Results

Infrared Spectroscopy. IR spectra of the Nd, Ho, Yb, and Lu solvent-phase compounds are compared in Figure 1 to the IR spectrum of the free TEMA ligand. The main region of interest in the middle infrared field is centered around the symmetric C═O stretching $\nu_{C=O}$ band between 1630 and 1590 cm^{-1}. All lanthanide complexes exhibit for $\nu_{C=O}$ (i) a decrease of the carbonyl stretching vibration frequency relative to that of the free ligand (Table 1) and (ii) a doubling of the carbonyl stretching band, giving rise to the $\nu'_{C=O}$ shoulder. The low-energy shift of $\nu_{C=O}$(complex) with respect to $\nu_{C=O}$(free TEMA) accounts for the coordination of the ligand to the lanthanide nitrate via the oxygen atom of the carbonyl group. It is due to a decrease of the force constant of the carbonyl bond when the oxygen atom is engaged in metal complexation. The $\nu'_{C=O}$ shoulder that appears upon complexation is consistent with previously published data on solid-state compounds $Ln(NO_3)_3$-(TMMA)$_2$ (TMMA = *N*,*N*,*N*′,*N*′-tetramethylmalonamide)[57] and

(51) Ankudinov, A. L.; Rehr, J. J. *Phys. Rev. B* **1997**, *56*, 1712.
(52) Piquemal, J. P.; Leroy, C.; Michalowicz, A. Unpublished program available on the LURE web site (www.lure.u-psud.fr), 1998.
(53) Newville, M.; Ravel, B.; Haskel, D.; Stern, E. A.; Yacoby, Y. *Physica B* **1995**, *208&209*, 154.
(54) Stern, E. A.; Newville, M.; Ravel, B.; Yacoby, Y.; Haskel, D. *Physica B* **1995**, *208&209*, 117.
(55) For documentation, see the FEFFIT web site: cars.uchicago.edu/∼newville/feffit/.
(56) Den Auwer, C.; Dognon, J. P.; David F.; Revel, R.; Hubert, S. To be submitted for publication.
(57) Vicentini, G. *J. Inorg. Nucl. Chem.* **1972**, *34*, 669.

Table 5. Method A Best-Fit Results in the Single-Shell Approximation (distances R (Å) between the Metal and the Oxygen Atoms of Both Nitrate Groups and TEMA Ligands and Debye−Waller Factors σ^2(Å^2)) of Region I Filtered EXAFS Oscillations for Complexes $M(NO_3)_3TEMA_2$ ($M = Nd^{3+}$, Eu^{3+}, Ho^{3+}, Yb^{3+}, Lu^{3+}, Am^{3+}) in Solvent Phase: Comparison with Averaged Method B[a]

	M					
	Nd	Eu	Ho	Yb	Lu	Am
M−O dist (Å)	2.54 ± 0.01	2.50 ± 0.01	2.44 ± 0.01	2.40 ± 0.01	2.39 ± 0.01	2.52 ± 0.01
Debye−Waller factor σ^2 (Å^2)	0.0021 ± 0.0001	0.0040 ± 0.0001	0.0021 ± 0.0001	0.0035 ± 0.0001	0.0006 ± 0.0001	0.0035 ± 0.0001
S_o^2	1.16 ± 0.05	1.32 ± 0.06	1.14 ± 0.05	1.25 ± 0.05	0.95 ± 0.05	0.97 ± 0.05
e_0 (eV)	0.45 ± 0.01	−0.05 ± 0.01	0.28 ± 0.04	−0.06 ± 0.01	0.46 ± 0.01	−0.57 ± 0.17
s	0.0012	0.0008	0.0062	0.0220	0.0102	0.0630
r	0.001	0.001	0.009	0.008	0.006	0.007
method B av M−O dist (Å)	2.53	2.48	2.43	2.39[b]	2.40[b]	2.50

[a] S_o^2 accounts for the product of the inelastic losses $\mathbf{S_0^2}$ by the errors in the amplitude functions, and s is the mean of the data standard deviation calulated in the most pessimistic way (mean, quadratic mean, or inverse quadratic mean), r is the "r factor" of the Round Midnight code.[50] [b] Average does not take into account the elongated M−O distance for comparison with method A results, for which the electronic parameters used do not account for this bond.

Table 6. Method B Best-Fit Results (Distances R (Å) between the Metal and the Oxygen Atoms of Both Nitrate Groups and TEMA Ligands and Debye−Waller Factors σ^2(Å^2)) of Region I Filtered EXAFS Oscillations for Complexes $M(NO_3)_3(TEMA)_2$ ($M = Nd^{3+}$, Eu^{3+}, Ho^{3+}, Yb^{3+}, Lu^{3+}, Am^{3+}) in the Solvent Phase[a]

	M					
M	Nd	Eu	Ho	Yb	Lu	Am
R−O(nitrate) dist (Å)						
◆	2.67 ± 0.01	2.63 ± 0.02	2.58 ± 0.02	2.57 ± 0.01	2.62 ± 0.01	2.69 ± 0.02
○	2.67 ± 0.01	2.58 ± 0.02	2.53 ± 0.02	2.51 ± 0.01	2.52 ± 0.01	2.64 ± 0.02
□	2.62 ± 0.01	2.55 ± 0.02	2.51 ± 0.02	2.46 ± 0.01	2.48 ± 0.01	2.55 ± 0.02
●	2.57 ± 0.01	2.53 ± 0.02	2.47 ± 0.02	2.79 ± 0.01	2.80 ± 0.01	2.53 ± 0.02
△	2.53 ± 0.01	2.49 ± 0.02	2.43 ± 0.02	2.41 ± 0.01	2.43 ± 0.01	2.49 ± 0.02
×	2.52 ± 0.01	2.45 ± 0.02	2.39 ± 0.02	2.38 ± 0.01	2.39 ± 0.01	2.47 ± 0.02
Debye−Waller factor σ^2 (Å^2)	0.0020 ± 0.0006					
R−O(ligand) dist (Å)						
▲	2.44 ± 0.01	2.39 ± 0.02	2.34 ± 0.02	2.29 ± 0.01	2.31 ± 0.01	2.42 ± 0.02
Debye−Waller factor σ^2 (Å^2)	$\sigma^2 = 0.0007 \pm 0.0006$					
S_o^2	1.01 ± 0.03	0.99 ± 0.07	0.96 ± 0.08	1.40 ± 0.07	1.28 ± 0.04	0.83 ± 0.03
e_0 (eV)	0.42 ± 0.28	−0.92 ± 0.62	−1.30 ± 0.74	−2.20 ± 0.48	−1.29 ± 0.35	−0.37 ± 0.37
s	0.0012	0.0008	0.0062	0.0220	0.0102	0.0630
r	0.017	0.018	0.023	0.014	0.004	0.005

[a] ◆, ○, □, ●, △, and × account for the six M−O distances of the three nitrate oxygen atoms; ▲ accounts for the averaged four M−O distances of the two ligand oxygen atoms. S_o^2 accounts for the product of the inelastic losses $\mathbf{S_0^2}$ by the errors in the amplitude functions, s is the mean of the data standard deviation calulated in the most pessimistic way (mean, quadratic mean, or inverse quadratic mean), and r is the "r factor" of the FEFFIT code.[55]

$Ln(NO_3)_3(DMDBMA)_2$ (DMDBMA = *N*,*N*′-dimethyl-*N*,*N*′-dibutylmalonamide)[58] but is still unexplained. It was, however, determined that the $\nu'_{C=O}$ shoulder does not belong to a nitrate vibration mode because it appears also with chloride neodymium TEMA complexes.

Although the identification of the nitrate ν_2 band (NO stretching) was not possible due to a strong absorption of the ethanol solvent in the 1100−1040 cm^{-1} region, the IR data in the 1300−1315 and 1465−1480 cm^{-1} ranges clearly indicate coordinated nitrate ions (in the local C_{2v} symmetry). The 180 cm^{-1} splitting between the stretching nitrate bands ν_4 and ν_1 is consistent with the presence of bidentate coordinated nitrate(s)[59] in all samples.

The far-infrared region is also of great interest, since the metal−oxygen stretching vibrations can be observed. By comparison with published data,[60,61] we assume that the strong and broad band ν_{Ln-O}, observed between 205 and 215 cm^{-1}, accounts for the Ln−O(TEMA) bond. This band is shifted toward higher energies as Z_{Ln} increases. This is consistent with an increase of the Ln−O(TEMA) force constant with Z_{Ln} and suggests a reduction of the metal to ligand bond length.

Although more noisy because of lower metal concentration, the IR spectrum of the Am complex shows the $\nu_{C=O}$ band at the characteristic energy for the coordinated ligand and compares well with the IR spectra of the lanthanide species.

X-ray Diffraction. Some structures of malonamide complexes of rare-earth elements (La^{3+}, Nd^{3+}, Yb^3), with a 1:1 or 2:1 ligand/metal ion stoichiometry, have previously been reported by some of us.[62,63] Two more references only are given in the 1998 release of the CCDC database,[64] in which the metal ion is bonded to four (Sm^{3+}, Er^{3+}) or five (La^{3+}) bidentate tetramethylmalonamide molecules, in which case one of them is monodentate, the counterion being in all cases PF_6^-.[65]

(58) Nakamura, T.; Miyake, C. *J. Alloys Compd.* **1995**, *225*, 334.
(59) Nakamoto, K. *Infrared and Raman Spectra of Inorganic and Coordination Compounds*, 3rd ed.; Wiley: New York, 1978.
(60) Medvedev, Y. N.; Lokshin, B. V.; Zaitzev, B. E.; Klemenkova, Z. S.; Spiridonov, F. M. *Russ. J. Inorg. Chem. (Engl. Transl.)* **1992**, *37*(5), 589.
(61) Brown, D. Actinide and Lanthanide Nitrates. In *Inorganic Chemistry*; Bagnall, K. W., Ed.; Butterworths: London, 1972; Series Two, Vol. 7.
(62) Byers, P.; Drew, M. G. B.; Hudson, M. J.; Isaacs, N. S.; Madic, C. *Polyhedron* **1994**, *13*, 349.
(63) Chan, G. Y. S.; Drew, M. G. B.; Hudson, M. J.; Iveson, P. B.; Liljenzin, J. O.; Skålberg, M.; Spjuth, L.; Madic, C. *J. Chem. Soc., Dalton Trans.* **1997**, 649.
(64) Allen, F. H.; Kennard, O. *Chem. Design Autom. News* **1993**, *8*, 31.
(65) Castellano, E. E.; Becker, R. W. *Acta Crystallogr., Sect. B* **1981**, *37*, 61, 1998.

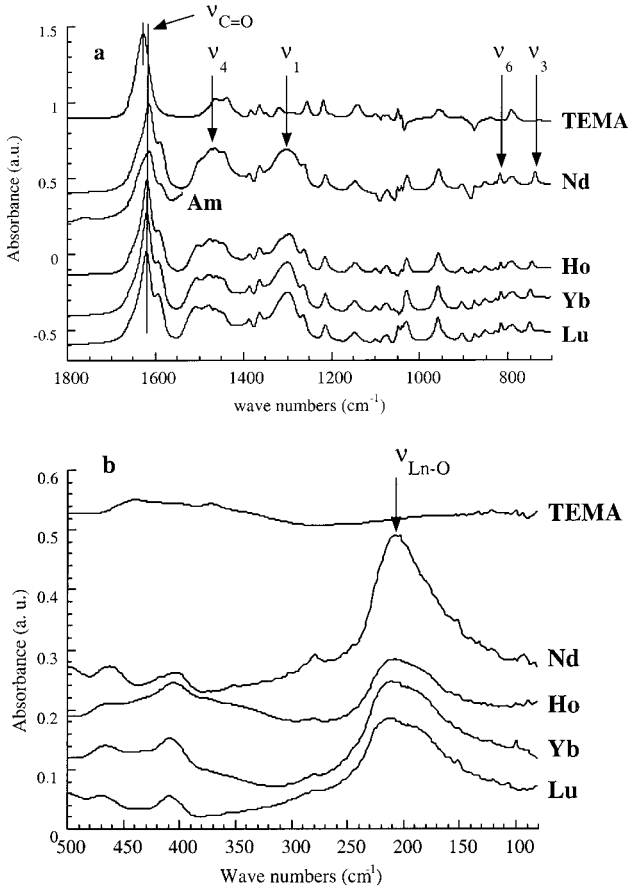

Figure 1. IR spectra of 0.2 mol/L $M(NO_3)_3(TEMA)_2$ solvent phase complexes (M = Nd, Ho, Yb, Lu) and 0.03 mol/L $Am(NO_3)_3(TEMA)_2$ solvent phase complex compared to the IR spectrum of free TEMA in ethanol. Spectra are shifted in ordinates for comparison. (a) Mid-IR region of the absorption spectra. Because of the large dilution of the Am complex, the scale has been multiplied by 1000 for this spectrum; (b) Far-IR region on polyethylene film.

However in the presence of a coordinating anion such as nitrate, the maximum number of malonamides per metal has been found to be 2. In the two compounds reported here, the bidentate TEMA ligand complexes the rare-earth nitrate with a 2:1 stoichiometry, giving complexes of general formula $M^{3+}(NO_3^-)_3(TEMA)_2$. The overall geometry of the molecules of complex **1** is the same as that already described in the case of $La^{3+}(NO_3^-)_3(TEMA)_2$,[62] the differences only originating from slight geometrical variations. We shall use the intraligand O···O distances and the values of the torsion angles defined previously[63] to compare the geometries of the TEMA central cores in the different structures (Table 4).

The monoclinic cell of **1** (Table 2) contains three crystallographically independent motifs (A−C). In each molecule, the metal ion is 10-coordinate, being bonded to two nearly coplanar bidentate TEMA ligands and three bidentate nitrate ions, two of them located on each side of the plane defined by the TEMA molecules and the third one crossing this plane, as illustrated in Figure 2. The terminal carbon chains of the ligands are affected by some disorder, seven atoms being distributed over two sites each (four for molecule B and three for C).

The Nd^{3+}−O(TEMA) (mean value 2.441(9) Å) and Nd^{3+}−O(nitrate) (mean value 2.59(6) Å) distances are smaller than in the La^{3+} complex previously reported[62] (2.53(5) and 2.70(8) Å, respectively), in agreement with the difference in ionic radii between the two ions. In addition, these values agree with those reported for other malonamide complexes of Nd^{3+}.[63] The

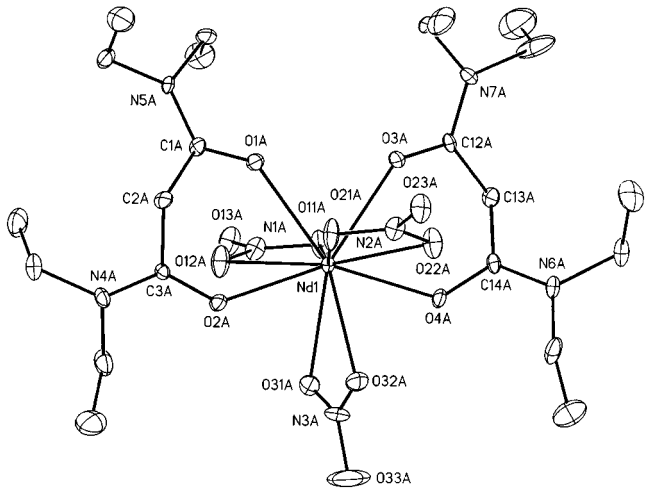

Figure 2. Molecular structure of $Nd(NO_3)_3(TEMA)_2$ with the atomic numbering scheme. Molecule A only is represented. Hydrogen atoms and disordered parts are omitted for clarity. Displacement ellipsoids are drawn at the 10% probability level.

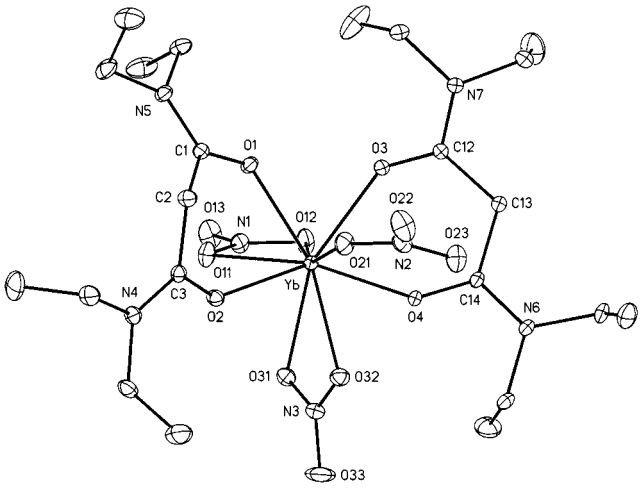

Figure 3. Molecular structure of $Yb(NO_3)_3(TEMA)_2$ with the atomic numbering scheme. Hydrogen atoms are omitted for clarity. Displacement ellipsoids are drawn at the 10% probability level.

O···O(carbonyl) distances in the TEMA moieties range from 2.726 to 2.850 Å, the mean value being 2.78(4) Å, to be compared with 2.89(2) Å for the structure of the La^{3+} complex previously published.[62] Slight differences are observed in the torsion angle values. As usual, all the C_{ext}−N−C−C angles (C_{ext} being the first carbon atom of the terminal chains) are near to the ideal values 0 or 180°, whereas the torsion angles involving the central atoms of the TEMA moieties can be rather far from this value. The O=C···C=O torsion angles indicate that, in molecule A of **1**, the TEMA central parts are more planar than in the other molecules, with values as low as 14.9 and 24.2°. Compound **1** presents an abrupt temperature-driven phase transition at about 192 K. Unfortunately, the low-temperature structure was not solved, seemingly due to twinning. Such a transition in a disordered structure is likely to be of the order/disorder type.

The principal difference between the molecular structure of the $Yb(NO_3)_3(TEMA)_2$ complex **2** and the above-discussed Nd^{3+} complex **1** is the change in the coordination number of the rare-earth ion. In contrast with **1**, the nine-coordinated complex **2** (Table 3), which has the same stoichiometry, contains one monodentate nitrate ion and two bidentate ones (Figure 3). The Yb^{3+}−O(TEMA) distances (mean value 2.290(7) Å) and the

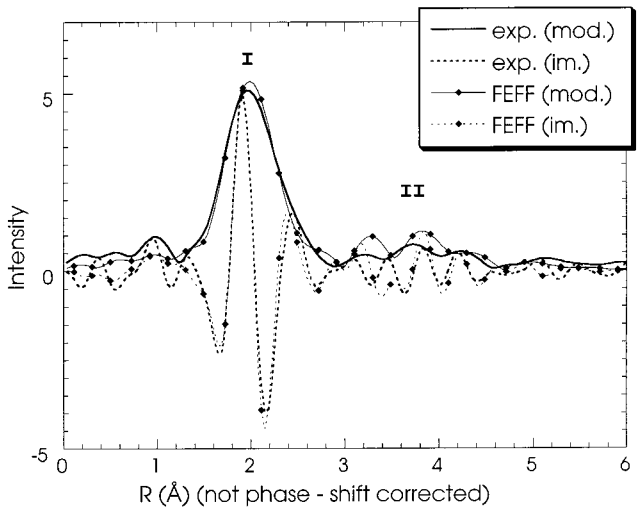

Figure 4. FT (mod. = modulus; im. = imaginary part) of the experimental and FEFF calulated EXAFS oscillations of molecule A in complex **1**, $Nd(NO_3)_3(TEMA)_2$.

Yb^{3+}−O(nitrate) distances for bidentate nitrate ions (mean value 2.47(6) Å) are significantly shorter than the corresponding distances for Nd^{3+} and La^{3+} complexes, in agreement with the difference in atomic radii. The Yb^{3+}−O distance for the monodentate nitrate ion (2.315 (2) Å) is shorter than for the bidentate nitrates but is still larger than the Yb^{3+}−O(TEMA) distances. The O···O distances in the TEMA molecules are also lower, and the central linkages of the TEMA ligands remain rather planar. No phase transition was found in **2** down to 163 K, in agreement with the absence of any disorder in this complex, containing only one crystallographically independent molecule in the orthorhombic cell.

One of the questions that should be addressed now is as follows: does complex **1**−complex **2** coordination sphere structural evolution apply to the solvent phase $M(NO_3)_3$-$(TEMA)_2$ entities?

EXAFS. Figure 4 compares the FT of the experimental spectrum to that calculated with FEFF of complex **1**. Detailed analysis of the calculated spectrum shows that the first peak **I** mainly accounts for all 10 oxygen contributions around the Nd atom, while the second part of the FT (region **II**) corresponds to a more complex multiple scattering part of the spectrum. Region **I** also contains 3 single-scattering M···N(nitrate) paths and several multiple-scattering paths of minor intensity. Thanks to phase opposition, all these contributions average to an insignificant term and region **I** is best represented by the 10 oxygen scattering paths. This phase cancellation phenomenon

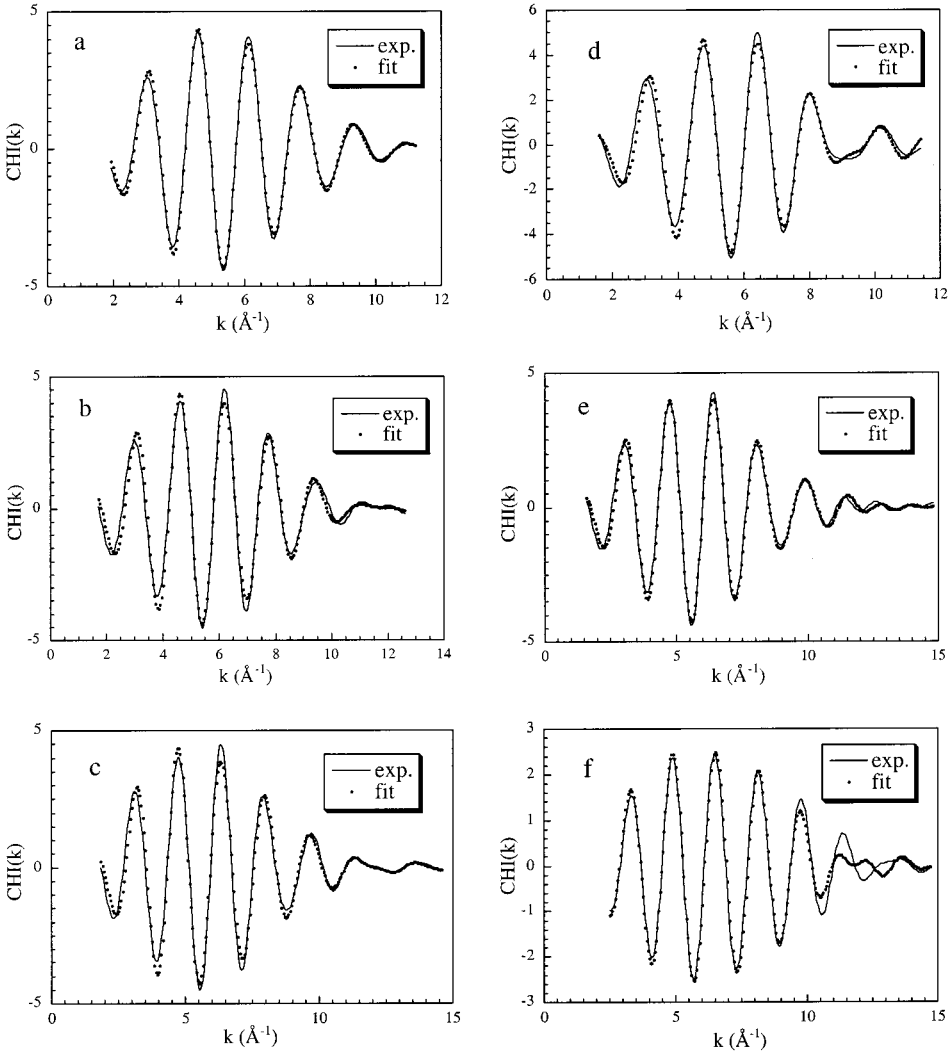

Figure 5. Experimental and fitted filtered EXAFS oscillations (back Fourier transformed EXAFS oscillations, real part) of complexes in the solvent phase: (a) $Nd(NO_3)_3(TEMA)_2$; (b) $Eu(NO_3)_3(TEMA)_2$; (c) $Ho(NO_3)_3(TEMA)_2$; (d) $Yb(NO_3)_3(TEMA)_2$; (e) $Lu(NO_3)_3(TEMA)_2$; (f) $Am(NO_3)_3(TEMA)_2$.

is even more striking in region **II**. FEFF simulation reveals that as many as 1100 paths (calculation carried out up to 7 Å) need to be considered to optimize the simulation of the FT modulus and imaginary parts of the experimental spectrum. Many of the FT features are due to multiple-scattering contributions involving both the carbon atoms of the ligand carbonyl groups and the nitrogen atoms of the ligand amide groups. Clearly, this is a very complex problem that cannot be treated the same way as in the case of region **I**. Attempts to reduce the number of significant paths to a reasonable amount for FEFFIT treatment failed, and only qualitative features can be drawn from this region.

Since region **I** is constructed from nondeconvoluted contributions, it is clear that precise analysis of the evolution of each of the 10 M−O contributions versus Z_{Ln} is hazardous and is only made possible by using electronic parameters (phase, amplitude, and electronic losses) extracted from the calculation of each scattering path, as explained in the Experimental Section. Therefore, region **I** has first been fitted as a one-shell contribution, and averaged M−O distances are given in Table 5. They show the decrease of the averaged Ln−O bond length from Nd^{3+} (2.54 Å) to Lu^{3+} (2.40 Å) ion according to the decrease in ionic radii along the series. Adjustment of the Am sample EXAFS spectrum shows that the averaged Am−O distance compares to the Nd−O distance (−0.02 Å). In a second experiment, the method B fitting procedure was employed (fits are presented in Figure 5). As a check, averaging the obtained 10 M−O distances compares well with the mean distance determined by the one-shell adjustment (±0.02 Å). Only the fit of the Lu compound seems to diverge (+0.01 Å compared to Yb) significantly. Considering each M−O path evolution across the series, the overall decrease of the bond distances is confirmed.

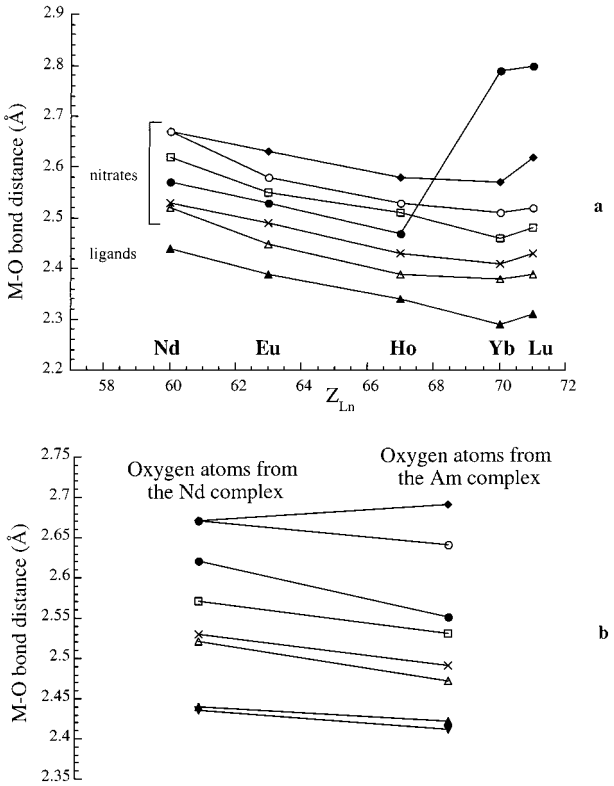

Figure 6. (a) M−O bond length in $M(NO_3)_3(TEMA)_2$ solvent-phase complexes (M = Nd, Eu, Ho, Yb, Lu, Am) (◆, ○, □, ●, △, and × represent the six oxygen atoms of the three nitrates; ▲ represents the averaged four oxygen atoms of the two ligands). (b) Comparison between the M−O bond lengths of the Am and Nd solvent phase complexes.

Discussion

The solid-state structure of **1**, $Nd(NO_3)_3(TEMA)_2$, is consistent with the expected stoichiometry of complexes of TEMA with the Nd^{3+} ion and shows the bidentate behavior of the malonamide ligands. The overall geometry appears well-established. However, disorder in the flexible parts of the TEMA molecule results in small geometric rearrangements in this class of compounds,[66] as for instance with the La^{+} cation. As is shown in Table 3, the Nd−O distances for the O atoms of the nitrate ions located on each side of the plane defined by the TEMA molecules are systematically larger than those for the ions crossing the plane, indicating a stress between the TEMA molecules and two nitrate ions in the coordination sphere of the Nd^{3+} ion. The increase in such stress for the complex with the smaller ion (Yb^{3+}) results in the change in coordination number and the occurrence of one monodentate nitrate ion.

In the solvent phase, all EXAFS adjustments have been carried out assuming as fitting initial conditions that 6 oxygen atoms are coming from the 3 nitrate groups and 4 oxygen atoms are coming from the 2 TEMA ligands, giving a nonfitted number of 10 oxygen neighbors. Note that the initial assumption of considering a structural model (based on complexes **1** and **2**) for the series is validated (i) by the fit goodness and (ii) by the coherence of the fit results. Obviously, the present analysis cannot distinguish between the 6 oxygen atoms of the 3 nitrate groups on one hand and the 4 oxygen atoms of the 2 ligands on the other hand. For instance, the 4 M−O(ligand) contributions were averaged, since no structural evolution was expected from the crystal structure, and this is verified by the low divergence obtained within these bond distances. The oxygen atoms of the nitrate groups were not averaged (unlike those of the ligands) in order to have access to complex **1**−complex **2** structural evolution, if any, in the solvent phase. It is, however, very likely that solvent molecules (water, alcohol) exchange with the metal coordination sphere, and thus only an average complex is seen by the EXAFS probe. In the solvent phase, the expected decrease of the averaged Ln−O bond length ⟨Ln−O⟩ for Ln = Nd, Eu, Ho, Yb, Lu given by the EXAFS measurements is in agreement with the reduction of the Ln^{3+} ionic radius r_{Ln}^{3+} when Z_{Ln} increases from Nd to Lu: ⟨Ln-O⟩ = 2.53 to 2.40 Å and r_{Ln}^{3+} = 1.107 (CN = 8) to 0.979 Å (CN = 8)[67] when Z_{Ln} = 60 to 71, respectively.[68] The evolution of each M−O path is presented in Figure 6a versus Z_{Ln}. Surprisingly, for the Yb and Lu cations, one of the oxygen atoms of one nitrate is moved away from the lanthanide first coordination sphere (to about 2.8 Å). This result compares to the solid-state structure of **2**, $Yb(NO_3)_3(TEMA)_2$, which is made up of one monodentate and two bidentate nitrates. However, in the solid-state structure of **2**, the two nonbonded oxygen atoms of the monodentate nitrate are located at 3.54 and 4.38 Å from Yb. The value of 2.83 Å given by EXAFS is therefore low for a nonbonded oxygen of a monodentate nitrate and can only be explained by a strong tilt of the NO_3^- entity away from the cation. In that sense, the lanthanide polyhedron may be viewed here as a 9 + 1-coordination mode instead of a 10-coordination mode for the Nd to Ho species. We were not able to confirm this trend by

(66) Thuéry, P.; Nierlich, M.; Charbonnel, M. C.; Den Auwer, C.; Dognon, J. P. *Polyhedron* **1999**, *18*, 3599.

(67) David, F. *J. Less-Common Met.* **1986**, *121*, 27.

(68) Ishiguro, S.; Umebayashi, Y.; Kato, K.; Takahashi, R.; Ozutsumi, K. *J. Chem. Soc., Faraday Trans.* **1998**, *94*, 3607.

the IR measurements, given the presence of the strong bands arising from the bidentate nitrates. We think indeed that very subtle steric hindrance relaxation effects do occur in the liquid phase compared to the solid state. Moreover, the presence of conformation equilibrium cannot be excluded, keeping in mind that polymorphism has been observed for this class of materials in the solid state. These results are, however, in agreement with the occurrence of one monodentate nitrate ion in the crystal structure of complex **2** and confirm the role of the steric stress around the cation as r_{Ln}^{3+} decreases.

To get rid of the ionic radius effect, results on the Am complex are compared to the one of the Nd complex since both cations have comparable ionic radii, i.e. $r_{Nd}^{3+} = 1.107$ Å and $r_{Am}^{3+} = 1.106$ Å.[67] These radii were extracted from measurements on oxide and halide compounds and poorly account for any f covalent character. Figure 6b presents both results on the same scale. Except for one oxygen atom of one nitrate, all other Am−O bonds are slightly shorter (but not significantly) than the Nd−O bonds. This is a major result that shows that the Am^{3+} coordination polyhedron has a structure similar to that of Nd^{3+} in these complexes.

Conclusion

In this paper, we describe the metal coordination sphere of a series of $M(NO_3)_3(TEMA)_2$ complexes (M = Nd, Eu, Ho, Yb, Lu, and Am) in the solvent phase. As a starting point of this work, the solid-state structure of the complexes $Nd(NO_3)_3(TEMA)_2$ and $Yb(NO_3)_3(TEMA)_2$ have been resolved. These structures show that, in both cases, two bidentate malonamide TEMA ligands are coordinated to the lanthanide ion through the carbonyl oxygen atoms. To complete the metal coordination sphere, Nd^{3+} is surrounded by three bidentate nitrate ions while Yb^{3+} is surrounded by two bidentate and one monodentate nitrate ion. This difference is attributed to the increase in the steric hindrance around the lanthanide ion when the ionic radius decreases from Nd^{3+} to Yb^{3+}.

In solution, from Nd^{3+} to Ho^{3+}, the metal coordination sphere was well fitted with three bidentate nitrate ions and two bidentate TEMA ligands, whereas for Yb^{3+} and Lu^{3+}, the best fit was obtained by a significant elongation of one of the Ln−O(nitrate) distances (2.8 Å), in agreement with the presence of a monodentate nitrate ion in the solid-state structure of $Yb(NO_3)_3(TEMA)_2$. In all cases, the Ln−O bond length decreases from Nd^{3+} to Lu^{3+} according to the reduction of the lanthanide ionic radii.

The coordination sphere of the Am^{3+} ion in $Am(NO_3)_3(TEMA)_2$ has also been investigated and compared to the one of the isostructural Nd^{3+} ions. The environment around Am^{3+} has been found to be similar to that around Nd^{3+} in $Nd(NO_3)_3(TEMA)_2$.

Acknowledgment. For their help and fruitful discussions, we thank Dr. J. P. Dognon and C. Berton, CEA Marcoule, DCC/DRRV/SEMP. Special thanks are given for financial support from NEWPART EC contract FI2W-CT91-0112 and Research Group PRACTIS (CNRS, CEA, EDF, ANDRA).

Supporting Information Available: Two X-ray crystallographic files in CIF format for compounds **1** and **2** and a figure giving the IR spectrum of the Am liquid-phase complex. This material is available free of charge via the Internet at http://pubs.acs.org.

IC990817X